Journal of Materials Chemistry B

ROYAL SOCIETY OF CHEMISTRY

PAPER

View Article Online
View Journal | View Issue

Cite this: J. Mater. Chem. B, 2024, 12, 9727

Highly stretchable nanocomposite piezofibers: a step forward into practical applications in biomedical devices†

Fatemeh Mokhtari,[a] Hui Yin Nam,[bc] Arjang Ruhparwar,[d] Raad Raad,[e] Joselito M. Razal,[f] Russell J. Varley,[a] Chun H. Wang[g] and Javad Foroughi*[deg]

High-performance biocompatible composite materials are gaining attention for their potential in various fields such as neural tissue scaffolds, bio-implantable devices, energy harvesting, and biomechanical sensors. However, these devices currently face limitations in miniaturization, finite battery lifetimes, fabrication complexity, and rigidity. Hence, there is an urgent need for smart and self-powering soft devices that are easily deployable under physiological conditions. Herein, we present a straightforward and efficient fabrication technique for creating flexible/stretchable fiber-based piezoelectric structures using a hybrid nanocomposite of polyvinylidene fluoride (PVDF), reduced graphene oxide (rGO), and barium-titanium oxide (BT). These nanocomposite fibers are capable of converting biomechanical stimuli into electrical signals across various structural designs (knit, braid, woven, and coil). It was found that a stretchable configuration with higher output voltage (4 V) and a power density (87 μW cm^{-3}) was obtained using nanocomposite coiled fibers or knitted fibers, which are ideal candidates for real-time monitoring of physiological signals. These structures are being proposed for practical transition to the development of the next generation of fiber-based biomedical devices. The cytotoxicity and cytocompatibility of nanocomposite fibers were tested on human mesenchymal stromal cells. The obtained results suggest that the developed fibers can be utilized for smart scaffolds and bio-implantable devices.

Received 25th July 2024,
Accepted 26th August 2024

DOI: 10.1039/d4tb01630k

rsc.li/materials-b

1. Introduction

As living standards rise, there is a growing focus on health management, especially for the elderly. Wearable and implantable medical devices play a key role in healthcare systems by enabling continuous monitoring, early disease detection, targeted treatments, personalized care, and improved connectivity. These devices aim to track physiological parameters before disease onset, enhancing quality of life and reducing pressure on healthcare facilities. However, current health-monitoring electronics are limited by their bulky design and reliance on external power sources, which restrict flexibility and mobility.[1] Therefore, advancing self-powered, personalized health diagnosis and treatment platforms is crucial for the future of healthcare.

As a forward step, wearable technology offers flexibility and reduces discomfort for continuous health monitoring, but concerns remain about biocompatibility, safety, long-term effects on the body, effectiveness, and efficiency.[2] Conductive polymers and piezoelectric materials are two key components in wearable technology and biomedical applications. Electrically conductive

[a] Carbon Nexus at the Institute for Frontier Materials, Deakin University, Waurn Ponds, Victoria 3216, Australia
[b] Department of Orthopaedic Surgery (NOCERAL), Faculty of Medicine, University Malaya, Kuala Lumpur 50603, Malaysia
[c] M. Kandiah Faculty of Medicine and Health Sciences, University Tunku Abdul Rahman, 43000 Kajang, Selangor, Malaysia
[d] Department of Cardiothoracic Transplantation and Vascular Surgery Hannover Medical School Carl-Neuberg-Str., 130625 Hannover, Germany
[e] Faculty of Engineering and Information Sciences, University of Wollongong Northfields Ave, NSW, Wollongong, NSW 2522, Australia
[f] Institute for Frontier Materials, Deakin University, Waurn Ponds, Victoria 3216, Australia
[g] School of Mechanical and Manufacturing Engineering, University of New South Wales, Sydney, NSW 2052, Australia. E-mail: j.foroughi@unsw.edu.au

† Electronic supplementary information (ESI) available: Movie S1 showed the development of piezoelectric textiles through melt-spinning and fabrication techniques for wearable technology applications. Movie S2 demonstrated the development of knitted piezoelectric textiles as a proof of concept for monitoring blood flow in vessels, muscle contraction, and airflow during breathing. Movie S3 demonstrated the performance of the braided structure during activity by presenting the assigned signal for mechanical loading/unloading through hand bending and finger tapping. See DOI: https://doi.org/10.1039/d4tb01630k

polymers have shown promise in delivering electrical stimuli, sensing, cell scaffolding, and tissue repair.[3] However, their biocompatibility and processability, such as their hydrophobic nature, limit cell compatibility, requiring further chemical modifications for better protein adhesion and bioactivity.[4] Electrical stimulation of these polymers for cell proliferation and differentiation (salivary,[5] nerve,[6] bone tissue[7,8]) requires an external power source. Despite successful *in vitro* tests on conductive polymeric scaffolds, clinical applications are still pending.

As bioelectronics typically interface with human bodies, piezoelectric materials raise significant concerns regarding biosafety and biocompatibility.[9] Unlike conductive polymers, piezoelectric materials can generate surface charges from small mechanical strains without external energy sources[10] making them suitable candidates for biomedical applications including cochlear implants, smart scaffolds, and pacemakers.[11,12]

Pacemakers are adjustable devices that generate electrical pulses, which can be temporary or permanent. Researchers are exploring energy harvesting techniques that could replace traditional batteries in pacemakers, creating a sustainable, self-powered system.[13] The focus is on converting biomechanical energy (from muscle movement, heartbeat, blood flow, or respiration) into electrical energy. Challenges include selecting safe, lead-free materials and designing compact, flexible structures (like zigzag or helical designs) that can generate sufficient power.[14] Current designs often exceed the ideal size (6 mm in diameter) for easy placement within the heart, making them impractical for real-world use. Most of the challenges are related to material selection, simple and practical design, size, and output power (1–10 μW).[15] Therefore, exploring all these demands is necessary.

Piezoelectric ceramics exhibit strong piezoelectric properties but are limited by their stiffness and brittleness.[16] Additionally, the use of toxic lead in PZT (lead zirconate titanate) and PMN-PT (lead magnesium niobate-lead titanate) raises biocompatibility concerns.[17] Piezoelectric polymers, such as PVDF, polyvinyl chloride (PVC), polyamides, liquid crystal polymers (LCPs), and parylene-C, are extensively used in biomedical applications requiring direct contact with the human body due to their flexibility, robust mechanical properties, and stability in varying environmental conditions.[18,19] PVDF and its copolymers, P(VDF-TrFE) and PVDF-HFP, are particularly considered for their remarkable piezoelectric effect and have been approved by the FDA for bioimplanted devices.[20] Consequently, piezoelectric polymeric materials have met the requirements of high integration, miniaturization, and low power consumption for wearable and biomedical technologies. Assembled in various forms like ultrathin films, electronic skins, fiber and e-tattoos, piezoelectric polymers not only mitigate the intrinsic mechanical mismatch between electronic devices and human skin but also greatly improve comfort and convenience. Piezoelectric polymers offer unique advantages for smart biomedical applications, such as high sensitivity, low detection limits, fast response, and minimal influence from body motion artifacts.

Wearable technology based on piezo polymers can convert biomechanical movements—like running, walking, breathing, and heartbeats—into electrical energy.[21,22] This technology addresses challenges in miniaturization, extends device lifespan, enables continuous operation, reduces surgical risks, and lowers costs by minimization the need for manual replacement and maintenance. To improve piezoelectric performance, material engineering strategies have been developed to enhance sensitivity, cyclic life, biocompatibility, and high-level processability. One approach to enhance the piezoelectric performance of these polymers is to incorporate different fillers. However, using biocompatible materials is crucial to avoid immune reactions, making it a top priority for creating safe and effective flexible, bio-functional devices.[23] To overcome these limitations, innovations in fabrication methods and structural modifications have offered practical and feasible ways to achieve high-performance piezoelectric polymeric materials. The most common technique for fabrication piezoelectric fiber is the electrospinning process. However, potential drawbacks must be considered when choosing this fabrication method. Electrospinning methods for fabricating scaffolds may not be optimal due to scalability challenges, time and energy consuming and tedious processes, and the requirement for precise control over fabrication parameters that affect fiber formation.[24] *In vivo* tests have shown that electrospun PVDF webs can provide uninterrupted power for a pacemaker while serving as sensor for blood pressure monitoring.[25,26] This represents significant progress compared to the first pacemaker implanted in a human body, which could only function for less than two years.[27] However, the use of aluminum foil as electrodes still limits their potential future applications.[28] Therefore, addressing the limitations of the electrospinning technique requires exploring alternative approaches.

Melt spinning is a process used to manufacture synthetic fibers. This method is widely employed in the textile industry to create fibers of various materials such as nylon, polyester, and polypropylene. It offers advantages such as high production rates, simplicity, and the ability to produce fibers with consistent properties suitable for a wide range of applications. Consequently, the fabrication of high performance PVDF and its composite fibers could be achievable through melt spinning. Adding different fillers such as barium-titanium oxide (BT) and reduced graphene oxide (rGO) can enhance piezoelectric properties of meltspun PVDF fibers. rGO, with its oxygen-containing functional groups, improves crystallinity and enhances piezoelectric performance by aligning fluorine atoms in the PVDF matrix. Meanwhile, BT, a dielectric material with piezoelectric properties, induces mechanical strain in the PVDF matrix, promoting the alignment of polymer chains into the β-phase and boosting piezoelectric response. The addition of BT nanofillers restricts the mobility of macromolecular chains, further improving the alignment and organization of PVDF chains in the beta-phase, leading to enhanced piezoelectric properties.[29]

Another challenge in using PVDF fibers for developing biomedical devices is their stretchability and flexibility of these fibers. Biomedical devices designed to capture energy require durability, flexibility, and stretchability to interact effectively with the body's soft tissues. The challenge of stretchability can

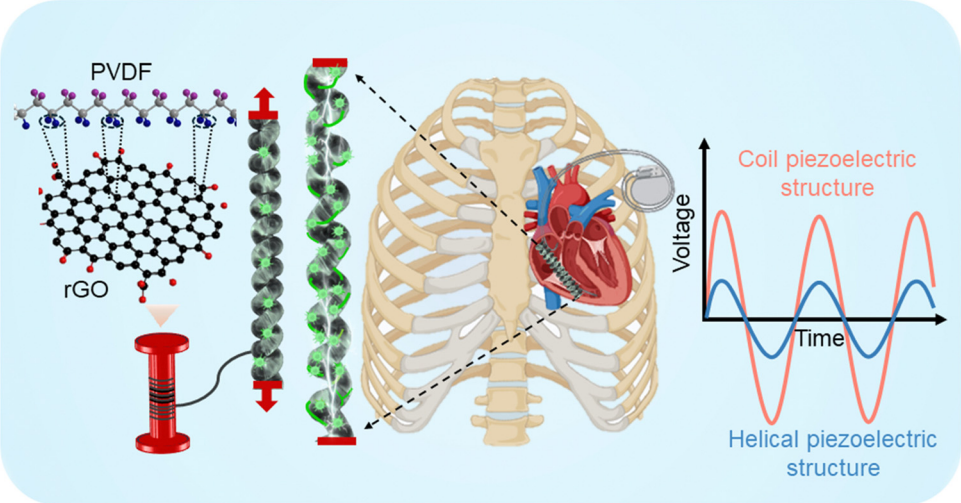

Fig. 1 Illustrating the capability of PVDF nanocomposite coils as smart scaffolds for biomedical applications, including pacemakers and stimulated scaffolds, proves to be an efficient method for promoting the proliferation or differentiation of diverse cell types.

be addressed in two ways: by exploring new stretchable piezoelectric materials such as hybrid composites, or by designing stretchable structures such as helical[30] or kirigami[31] structures. Research on stretchable structures and self-powered piezoelectric sensors for biomedical applications is limited and mostly at the prototype stage. Our work aims to address this knowledge gap by exploring both piezoelectric composition and fiber structures in biomedical applications.

Here, we present a novel approach for manufacturing flexible and stretchable piezoelectric structures using functional materials with biocompatibility. These structures have the potential to convert mechanical energy from biomechanical sources into electrical energy, making them suitable for applications such as wearable sensors for human motion detection, bio implanted devices, and intelligent scaffolds for tissue and nerve stimulation (Fig. 1). High-performance nanocomposite fibers were fabricated through a melt spinning process using PVDF, PVDF/barium-titanium oxide (BT), and PVDF/rGO piezoelectric materials. The piezoelectric performance of various structures, including braid, knitted, woven, and coil, is compared and discussed in terms of their potential for biomedical applications. Additionally, the cytotoxicity and cytocompatibility of nanocomposite fibers in two stretchable structures—coil and knitted—were tested on human mesenchymal stromal cells. The results demonstrate their potential as alternative materials for smart biomedical systems.

2. Results and discussions

2.1. Morphological characteristics and microstructural analysis of piezoelectric nanocomposites fibers

PVDF includes at least four different crystalline phases, having the non-polar α phase and polar β, δ and γ phases. The PVDF β-phase exhibits the most robust piezoelectric response, thanks to its parallel dipole moment alignment.[32] Therefore, to improve PVDF piezoelectricity for practical use, it is essential to enhance the polar β-phase volume fraction.[33] Nanomaterial fillers including piezoceramic BT with mean diameter of 50 nm (10 wt%)[34] and conductive rGO (0.5 wt%)[35] after concentration optimization are incorporated into the PVDF, along with post-treatment process of mechanical stretching with the a ratio of three and thermal annealing at 80 °C to enhance β-phase formation in meltspun fibers in diameter of ∼170 μm (see Movie S1 in the ESI† for more details).[34,36]

The PVDF α phase exhibits FTIR absorbance peaks at 764 and 975 cm^{-1}. Strong vibration β-phase peaks are at 840 and 1275 cm^{-1} (ref. 37) are observed in melt-spun fibers after cold drawing process (Fig. 2a). The increased β phase formation occurred within the coil structures, likely attributed to enhanced stretching and alignment of dipoles along the fiber axis during coil manufacturing. The PVDF/rGO nanocomposite coil exhibited the highest β phase formation, showcasing a 52% improvement compared to its untwisted filament (Fig. 2b).[35] rGO contains various oxygen-containing functional groups, such as hydroxyl, carboxyl, and epoxy groups, located on its edges and basal planes. These functional groups form strong hydrogen bonds with the fluorine groups in PVDF, promoting the alignment of fluorine atoms both parallel and perpendicular to the polymer chain.[38] This alignment facilitates the phase transition from the α-phase to the β-phase, stabilizing the polar phase and enhancing energy harvesting performance through the formation of micro-capacitors within the polymer composite.[39] Since the electroactive phase content does not guarantee the piezoelectric activity of nanocomposite fibers, PFM studies and the dielectric properties of the fibers were also evaluated in our previous works to optimize filler concentration and the fabrication process.[34,36] The coil fabricating technique was explained in our previous work.[35]

The tensile strength and Young's modulus of the as prepared PVDF/rGO nanocomposite fiber exhibit a remarkable enhancement of 163%, and 208% respectively, compared to pure PVDF fiber (Fig. 2c).[35]

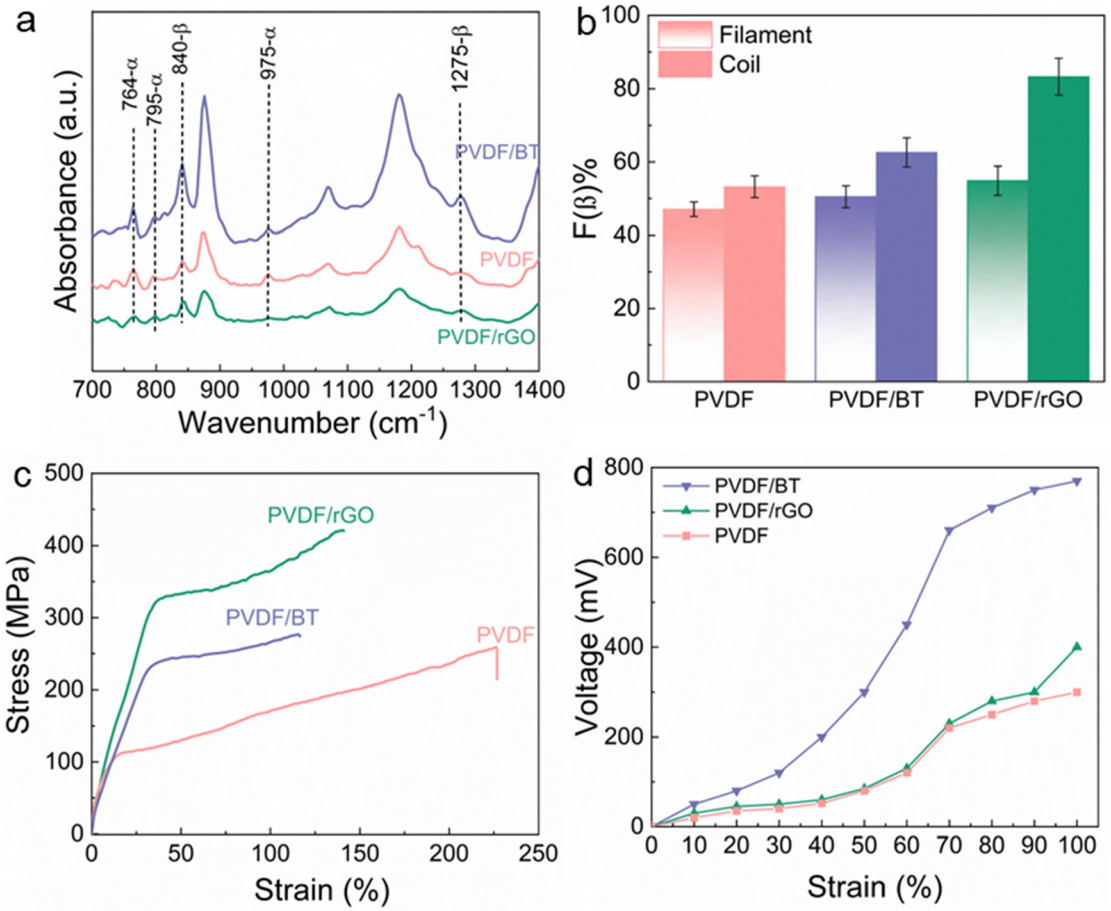

Fig. 2 PVDF and its nanocomposite fibers characterization: (a) FTIR spectra and (b) comparison of β phase formation in fiber and coil structures,[35] (c) mechanical stress–strain curves,[35] (d) maximum output voltage of coil nanocomposites at different levels of strain.[35]

Table 1 Mechanical properties of PVDF and its nanocomposites fiber

	Young's modulus (MPa)	Tensile strength (MPa)	Elongation at break (%)
PVDF	670	258	226
PVDF/BT (10 wt%)	1593	276	117
PVDF/rGO (0.5 wt%)	1396	420	141

One of the key factors contributing to better mechanical properties in composite structures is the homogeneous dispersion of fillers, along with strong interfacial interactions between the filler particles and the polymer matrix (Table 1). Fillers act as temporary cross-linkers between the polymer chains, creating localized regions with enhanced tensile strength and modulus. These results confirm the reinforcing role played by BT (10 wt%) nanoparticles in the PVDF fibers.[40]

The carbonyl functional groups present in graphene oxide nanosheets enhance the compatibility between PVDF and rGO. This results in a homogeneous dispersion of rGO within the PVDF matrix and efficient interfacial stress transmission at an rGO content of 0.5 wt%. Consequently, the mobility of the polymer chains is reduced, leading to improved mechanical performance in the PVDF/rGO nanocomposite fibers compared to those of PVDF/BT.[41]

Fig. 2d shows that subjecting the nanocomposite coils to a 100% strain results in the generating a maximum output voltage of 800 mV for PVDF/BT coil fiber.[35] Coil structures are the preferred choice for stretchy fabrics designed to monitor the movement of robots, humans, and artificial skins, offering unrestricted stretching capabilities in any scenario. The performance highlighted above demonstrated the promising properties of nanocomposite fibers in terms of mechanical strength and β phase formation. Furthermore, it illustrates how the coil fabrication process enhances piezoelectric performance, as observed in our previous studies.[34,35] As a forward step, we describe the capability of these nanocomposite fibers for development and use in biomedical applications.

2.2. Mechanical stimuli of nanocomposite piezoelectric fibers

The fabricated nanocomposite piezofibers are presented in four different structures as wearable and implantable biomedical devices for smart healthcare technology, as described in Table 2. These structures, owing to their flexibility, stretchability, low cost, miniaturization, and provision of battery-free features by generating voltage, would offer an eco- and patient-friendly platform for real-time and long-term healthcare applications. The braiding design features hybrid piezoelectric fibers capable of

Table 2 Performance comparison of nanocomposite piezoelectric fibers in different structures

Structures	Electrodes	Exitation method	Power and signals	Sensitivity (V N^{-1})	Fabricated structures	Ref.
Braid	One single silver coated nylon yarn as the core and six braid ones as the shell	Applied pressure of 0.023 MPa	380 mV, 29.62 μW cm^{-3}	4	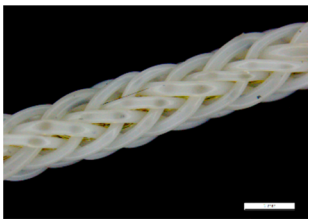	36
Circular knited	Silver coated fabric inside and outside of the tube	Periodic impact pressure of 0.023 in frequency of 1 Hz	4 V, 87 μW cm^{-3}	10	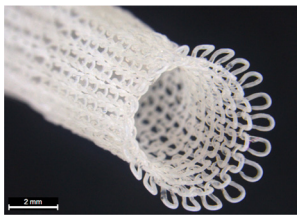	34
Woven	Silver coated fabric sandwiched the structure from top and bottom	Periodic impact pressure of 0.023 in frequency of 1 Hz	1 V, 36.2 μW cm^{-3}	3	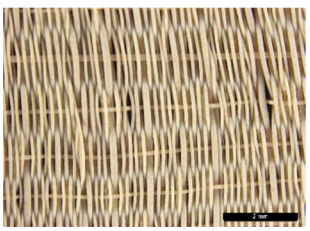	34
Coil	Silver coated nylon on both ends	Stretch up to ≈100% strain by applying 60 MPa stress	1.3 V, 0.42 μW cm^{-3}	1.3	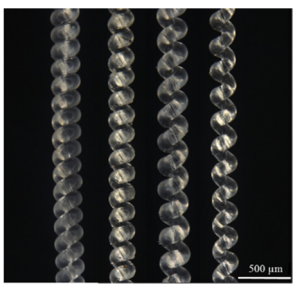	35

producing a remarkable output voltage when subjected to compression or bending. The developed triaxial braided structure enables poling between the inner and outer electrodes (applying 20 kV at a temperature of 80 °C for a duration of 10 minutes) where the braided PVDF fibers are as an intermediate structure.[36] This design supplies a high-power density of 29.62 μW cm^{-3}, a significant improvement of approximately 1600% compared to previous piezoelectric textile designs. This compact structure demonstrates remarkable durability, enduring thousands of cycles with up to 50% strain without performance decline.[36] The circular knitted structure, due to its high stretchability, is a favourable choice for biomedical devices. The circular knitting pattern allows for the smooth integration of conductive fiber-based electrodes within the triaxial structure, including both inner and outer electrodes. This integration has the potential to greatly enhance charge collection and energy conversion efficiency. This structure is able to generate a maximum voltage of approximately 4 V with a high sensitivity of 10 V N^{-1} under finger tapping pressure, which is about six times higher compared to recent reports.[35] This structure also demonstrates higher sensitivity compared to woven (3 V N^{-1}) and braid structures (4 V N^{-1}).[36] This circular structure is suitable for monitoring blood flow in vessels, muscle contraction, and airflow during breathing (see Movie S2 in the ESI† for more details).

A woven energy-generating structure capable of producing a maximum output voltage of 1000 mV and storing 36.2 μW cm^{-3} of energy during periodic compression. It is designed for integration into high-bend areas such as elbows, wrists, and knees. The output voltage is adjustable, ranging from 300 mV for walking to 1000 mV for running (at a frequency of 1.2 Hz). This wearable generator can charge a 10 μF capacitor in 20 seconds, reaching a maximum voltage of 25 mV.[34] As shown in our previous work, this structure demonstrated good capability in human motion detection, including bending knee angles of 45 and 90 degrees, making these sensors useful for real-time precise healthcare applications.[42]

The transformation of nanocomposite fibers into a coiled structure was achieved through precise twisting and coiling methods. The coiled piezofiber energy harvester presents itself as a promising option for various applications in energy

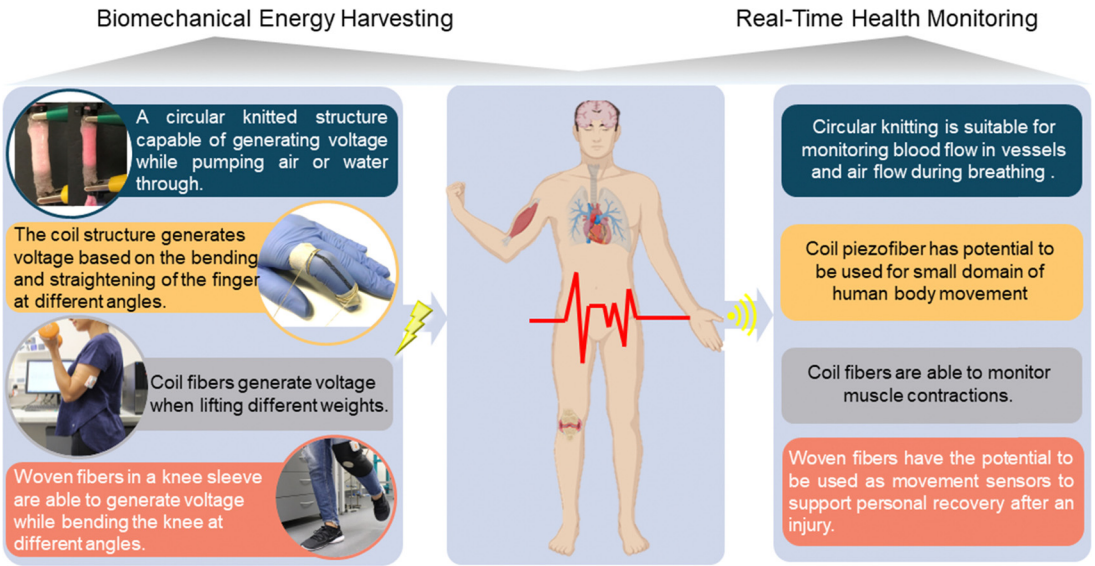

Fig. 3 Demonstrating the performance of hybrid piezoelectric fibers in various structures and proposing their potential applications for biomedical devices, including powering IoT devices and real-time health monitoring.

harvesting devices, especially within wearable smart garments and self-powered wireless sensors integrated into clothing for human health monitoring. Additionally, it serves as a smart scaffold for cell culturing, thanks to its ability to generate 1300 mV of energy during 100% strain.[35] The energy generators and sensors made from nanocomposite fibers are ideal for applications prioritizing energy harvesting, stretchability, and exceptional electromechanical properties. These coil structures can enhance output voltage by adjusting the original fiber diameter, length, and quantity.[35]

Fig. 3 demonstrates the application of these nanocomposite fibers in energy harvesting from human body movement, which can be considered a clear-cut solution for powering wireless terminals including sensors and internet of things (IoT) technologies, using non-polluting (clean) energy, as presented in our previous works.[34–36] This serves as proof that these structures, due to their high performance, flexibility, stretchability and easy fabrication process, are ideal for use as smart scaffolds for biomedical application (see Movie S3 in the ESI† for more details).

2.3. Cytocompatibility of the fabricated smart scaffolds

Stretchability is an essential property for wearable devices to accommodate diverse strains when interfacing with soft tissues or organs. Hence, among the fabricated structures, coil and circular knitted structures were evaluated for their suitability in biocompatibility and cell culturing studies. Since conductive fillers like rGO play a crucial role in transferring piezoelectric signals to tissues,[43] as prepared PVDF/rGO nanocomposites fiber was chosen for further evaluation among the various fillers. In the case of water absorbance, rGO presents a trade-off between graphene and GO, as it retains some epoxide and hydroxyl groups, which enhances its compatibility with most polymers and improves its electrical properties.[44] Incorporating rGO into PVDF improves its β phase fraction, wettability and hydrophilicity, benefiting cell adhesion and proliferation, which is favourable for biocompatibility and bioapplications.[45] The surface properties of biomaterials also greatly influence cell adhesion. Incorporating rGO into PVDF enhances its surface hydrophilicity, leading to decreased contact angles, indicating improved hydrophilicity.[46]

These piezoelectric structures convert mechanical stress into electrical signals. When piezoelectric materials are used as scaffolds, they can perfectly mimic the environments of natural tissues in generating voltage such as bone, nerve, and the cochlea, stimulating tissue regeneration, healing, and diagnosing medical problems.[47] Therefore, piezoelectric materials have been studied further for exploration in tissue engineering applications. Fig. 4a shows a schematic illustration of the proposed piezoelectric coil structure undergoing mechanical stimulation by longitudinal stretching. It is suggested that the resultant voltage generated by this structure will promote cell growth. Fig. 4b and c show skeletal muscle cells grown on PVDF/rGO fiber and coil after 4 days, indicating that adding rGO to both scaffolds (fiber and coil) does not induce cytotoxicity in human skeletal muscle cells.

Although graphene, graphene oxide, and reduced graphene oxide materials are commonly studied and used for *in vitro* cell culture and *in vivo* animal models, it is vital to assess the cytocompatibility of the fabricated materials as graphene materials may contain toxic chemical residuals for their synthesis.[48]

While it is common and established that bone marrow-derived mesenchymal stromal cells are used in many studies and therapies, harvesting bone marrow is an invasive and painful procedure with a low yield of stem cells. Therefore, other sources of stem cells such as human mesenchymal stromal cells derived from adipose tissue (AD-MSCs) were

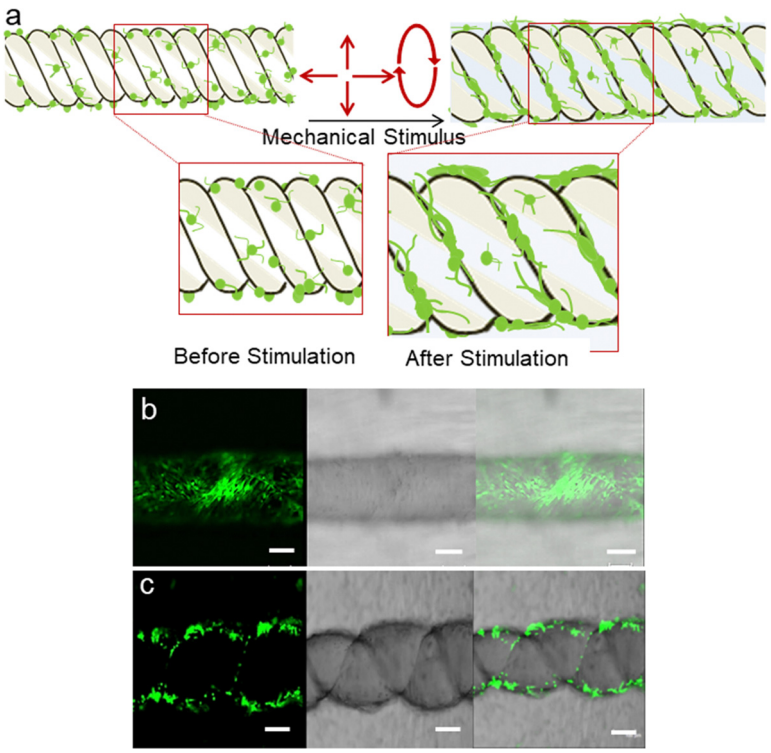

Fig. 4 (a) Schematic illustration depicting cell attachment and growth on coil structure under mechanical stimulation. Skeletal muscle cell attachment and proliferation on fibers after 4 days of differentiation. (b) PVDF/rGO fiber and (c) PVDF/rGO coils. Scale bars represent 100 μm.

chosen for this study owing to their abundance, easy accessibility, and good capacity for *in vitro* proliferation and differentiation,[49,50] with a major focus on their clinical applications to treat various musculoskeletal ailments.[51] AD-MSCs have been reported to migrate to damaged sites, providing a good platform for the development of regenerative medicine and other biomedical fields. Many previous studies have showed that graphene and its derivatives offer many advantages, including excellent electrical conductivity, mechanical strength, and good elasticity, which benefit biological properties.[52,53]

In our study, the isolated AD-MSCs attached to the culture flask and displayed spindle-shaped morphology (Fig. 5a). The isolated cells were well-characterized by flow cytometric analysis (>95% for CD44, CD90, CD105, while <2% for CD14, CD45, HLA-DR) and induction of trilineage (osteogenic, adipogenic, chondrogenic) differentiation assay. Based on the results of cell identification analyses, it was confirmed that the isolated stem cells were MSCs, following the minimal criteria defined by the mesenchymal and tissue stem cell committee of the international society for cellular therapy (ISCT). The passage-3 AD-MSCs were used in this study as they appeared more homogeneous after cell passaging. It is reported that effective application of MSCs in disease treatment relies on the production of relatively homogeneous cell population.[54]

Cytocompatibility tends to be defined by two main factors: cell viability and activity/proliferation in the presence of the material. *In vitro* cell proliferation and viability measured using AB assay are shown in Fig. 5b and c. Overall, even though a significant difference was not observed between the samples (absence or presence of rGO), the samples had similar percentage AB reduction levels, suggesting high cell viability and minimal cytotoxicity. The pattern is apparent when the cells seeded in the coil structure increased significantly on day 14 compared with day 1. It seems that the PVDF coil structure containing rGO into the did not impair cellular behavior but enhanced cell proliferation over the duration of the culture, similar to the pattern shown in the PVDF coil in the absence of rGO. This finding is further proven by comparing the changes in cell morphology of the samples surface, as shown in Fig. 6a–d, which shows that cells adhered and elongated on the scaffolds.

Observation of the structures under FESEM confirmed the presence of attached cells on three-dimensional structure of the scaffolds. The images revealed that the cells attached properly on the scaffolds and expanded to form cell layer. After 14 days of culture, the cells were able to penetrate and proliferate throughout the entire scaffold architecture, forming a network of interconnected cells, particularly on the rGO coil structure scaffold. The FESEM images further confirmed the results of alamarBlue assay, where the cells grew and survived on the PVDF/rGO coil fiber scaffold. The spreading and distribution of the cells on the scaffold surface were analysed using confocal microscopy. The images of the fiber scaffold demonstrated the distribution of cells on the scaffolds (blue spots) (Fig. 7a and b).

It is postulated that our current biological findings may be due to the rGO itself which has been found to improve

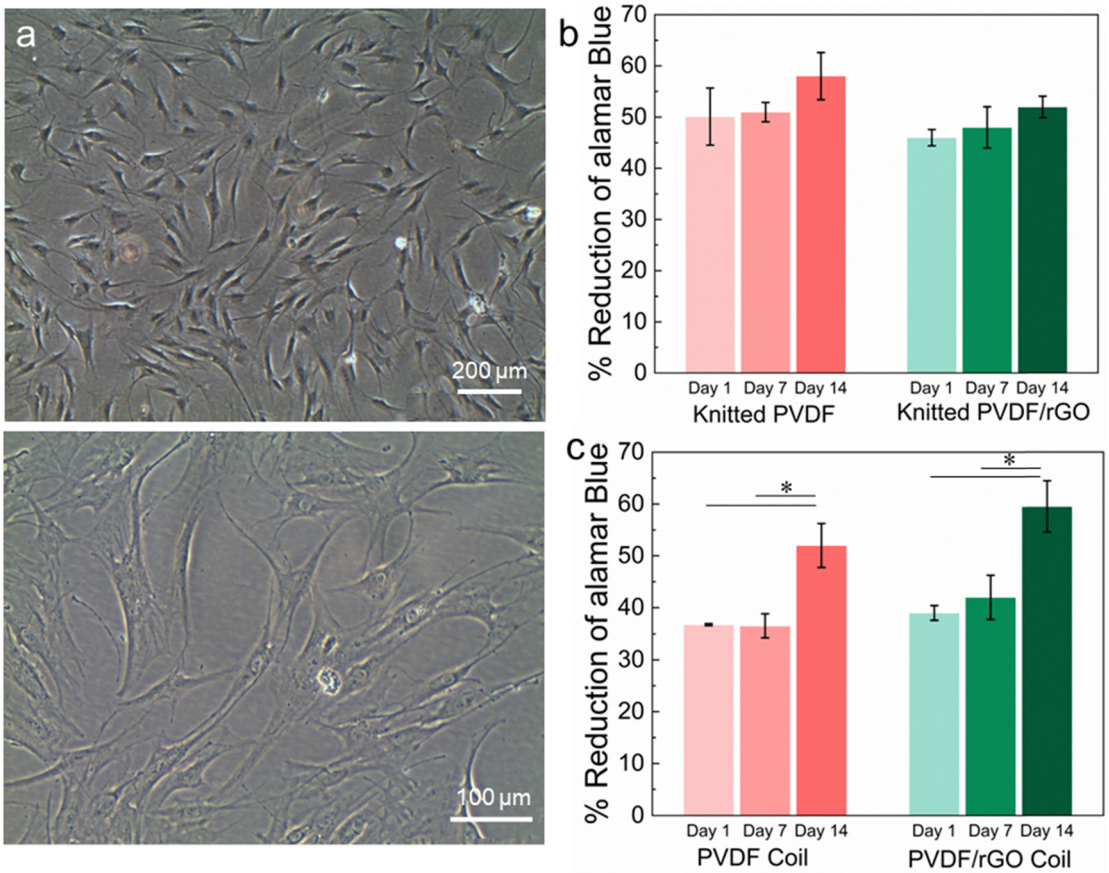

Fig. 5 *In vitro* cell proliferation and viability. (a) Phase contrast image of cultured passaged-3 AD-MSCs at different magnification (×40, ×100) showed homogenous fibroblastic shape. (b) The MSCs proliferation and viability on PVDF and PVDF/rGO knitted fiber assessed by AB assay on days 1, 7 and 14, indicating minimal cytotoxicity. (c) The MSCs proliferation and viability on PVDF coil and PVDF/rGO coil assessed by AB assay on days 1, 7 and 14. Significance ($p < 0.05$) was indicated with an asterisk (*) which compared between different group. $N = 4$, $n = 3$. Error bar = ±SD.

biocompatibility when combined with PVDF in the coil structure. The enhancement in output performance could be mainly attributed to the fact that rGO is able to induce the formation of β phase in coil fibers (shown in our earlier result),[35] enhancing electrical charges that could significantly improve cell behaviour. The good interface bonding between PVDF and rGO on twisted topography also contributed positively to cell growth by enhancing their mechanical-electrical conversion efficiencies. Our finding is supported by a study[38] which reported that cell behaviour could be improved by incorporate GO with PVDF as reinforcements, forming strong interaction with PVDF chains. Another study suggested that the incorporation of GO nanosheets into PVDF scaffold simultaneously enhanced β phase fraction, piezoelectricity and electrical conductivity of all nanocomposite scaffolds, thereby promoting cell proliferation.[46] Physical cues such as scaffold surface topography, roughness construction and incorporation of nanofiller guide cell behaviour.[55,56] Some of our previous studies have shown that cells interact with their niche and *via* adhesion molecules, which eventually transduce mechanical or physical cues to maintain their homeostatic function, through mechanotransduction processes.[57,58] The results of our current study indicate that the coil structure is able to enhance cell–cell interaction, which are vital for directing stem cell fate, and can be an invaluable tool for biomedicine applications. This has prompted us to investigate the osteogenic differentiation of AD-MSCs on the knitted fiber scaffold, as bone exhibits piezoelectric properties.[59] This phenomenon could be explained by the fact that bone exhibits piezoelectric properties due to the highly oriented and patterned structure of collagen, and collagen's ability to respond to mechanical loads.[60] This provided us with a baseline of cells fate on scaffolds with rGO integrations.

Additionally, the osteocalcin and alizarin-red results as shown in Fig. 7c–d demonstrated that the knitted fiber structure did not direct MSCs towards osteogenic differentiation. We hypothesize that stem cell osteogenic differentiation can be modulated on our fabricated coil fiber scaffold by applying mechanical stimulation.

3. Conclusion

In conclusion, this paper presents a comprehensive exploration of high-performance piezoelectric materials, specifically PVDF

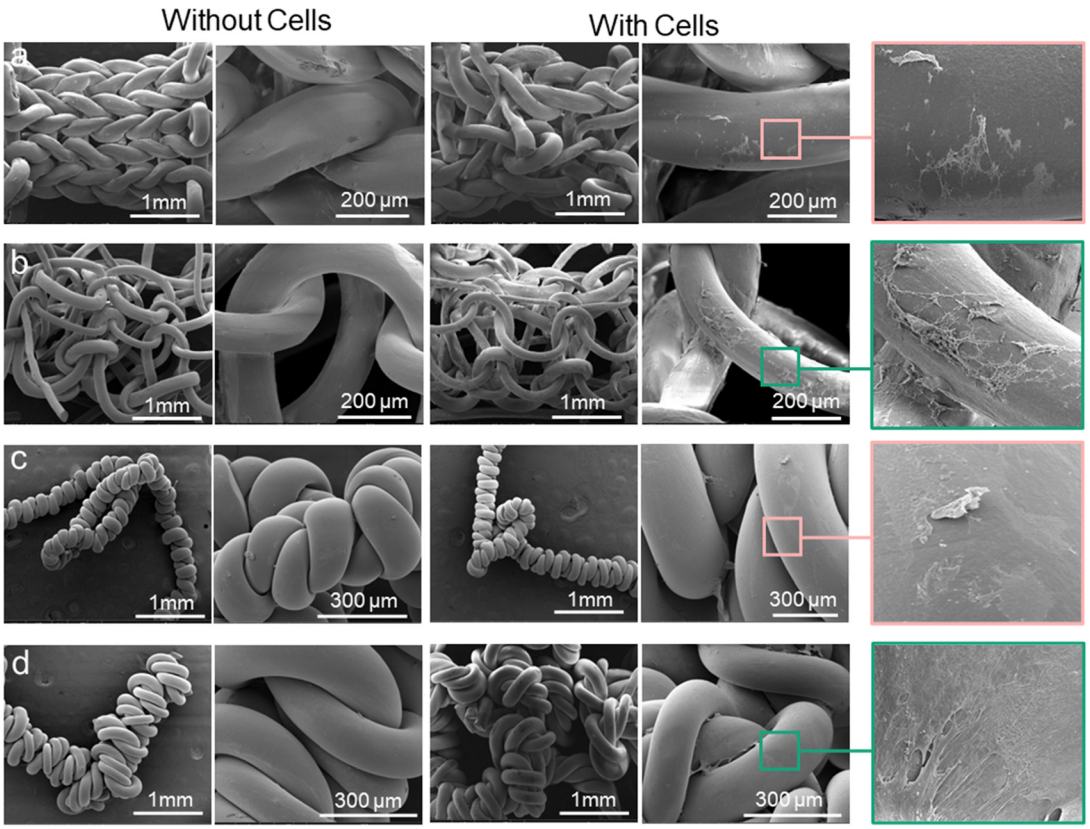

Fig. 6 The representative images of cells on scaffolds by microscopic imaging. (a) Scanning electron microscopy representative images of different scaffold without and with MSCs on day 14. FESEM images depicting cell attachment and spreading on all fibers obviously on (a) PVDF knitted fibers, (b) PVDF/rGO knitted fibers, (c) PVDF coil structure, (d) PVDF/rGO coil fibers.

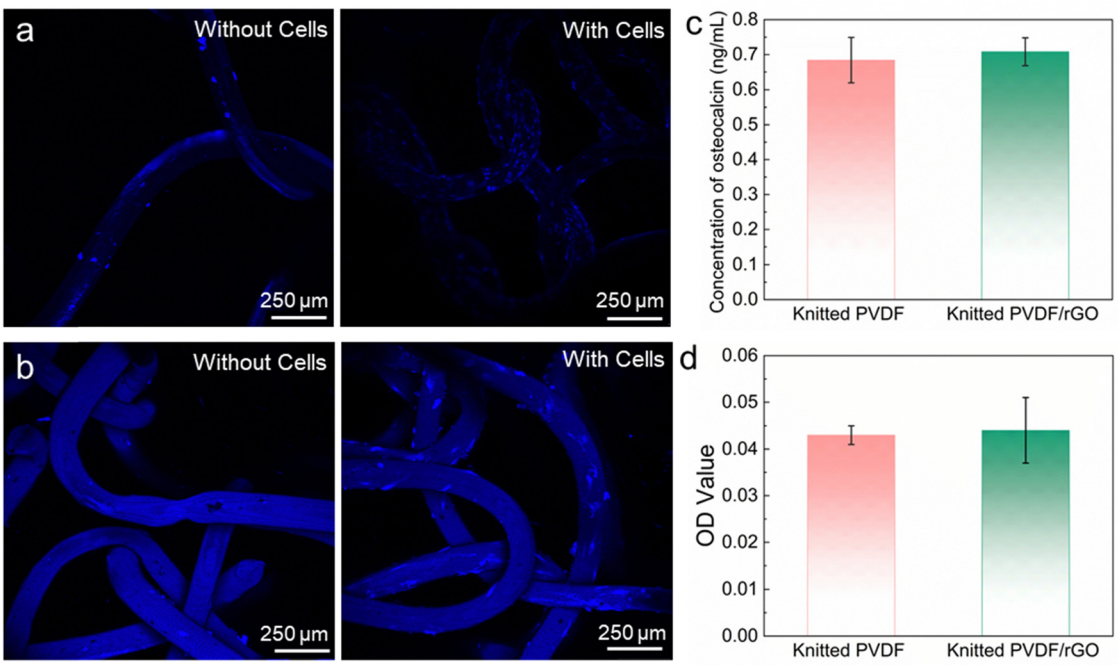

Fig. 7 FESEM image of knitted structure of (a) PVDF, (b) PVDF/rGO (the blue dots indicate distribution of the cells on scaffold). *In vitro* osteogenic expression assay. (c) Osteocalcin (OCN) production on the different fiber scaffolds at the day 14, (d) the matrix mineralization was determined *via* optical density (OD) level with alizarin red-S staining quantitative analysis. Both results expressed no difference between the group, either with or without rGO. $N = 4$, $n = 3$. Error bar = ±SD.

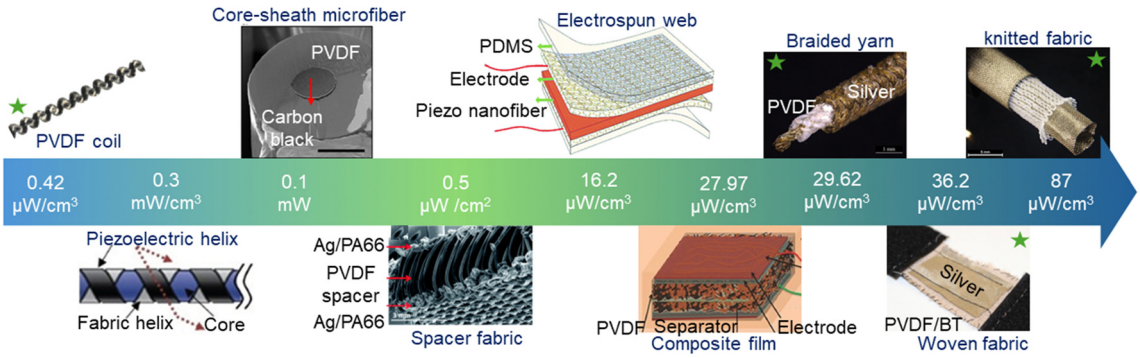

Fig. 8 Comparison of the structures and output power of the fabricated PVDF-based generators (indicated by a green star) with previously reported studies.[61–65]

and its nanocomposites with BT and rGO, used in the fabrication of melt-spun fibers. These fibers were creatively shaped into various structures, including knitting, braiding, weaving, and coil configurations (Fig. 8).

These versatile structures offer a promising solution to the challenge of long-term energy supply for electronic implantable biomedical devices, particularly cardiac pacemakers. A micro-engineering approach employing geometric design was introduced to develop self-powered flexible piezoelectric coil and knitted generators, addressing the limitations of traditional piezoceramics and polymers. The inherent high stretchability of knitted and coil structures enables them to generate voltage with high sensitivity upon mechanical stimulation. Consequently, these structures emerge as excellent candidates for smart scaffolds, satisfying specific requirements to induce human cell response at physiological levels while maintaining biocompatibility and performance integrity.

In vitro experimentation confirms the biocompatibility of these structures, with AD-MSC cells demonstrating robust attachment and growth on the coil structure due to its close-loop configuration. Overall, the results of this study offer a promising avenue for the development of flexible nanocomposite piezoelectric fiber generators and sensors based on PVDF nanocomposites. These materials serve as the foundation for non-toxic, biocompatible, and eco-friendly self-powered bioelectronics, facilitating the advancement of wearable devices for real-time healthcare monitoring, smart scaffolds for tissue repair and regeneration, and implantable biomedical applications.

4. Experimental section

4.1. Materials

Poly(vinylidene fluoride) (PVDF) powder was supplied by Solvay Soleris (Milan, Italy) under the commercial name Solef 6010. Sigma Aldrich Company (China) supplied cubic barium titanate nanoparticles with an average diameter of 50 nm and a purity of 99.9%. Dimethylformamide (DMF), with a purity of greater than 99.8%, was purchased from Merck and was used as the solvent. Our previous works comprehensively explained the procedure for synthesizing rGO.[66]

Dulbecco's modified Eagle medium (DMEM), foetal bovine serum (FBS), L-glutamine 2 mM, Roswell Park Memorial Institute (RPMI 1640), 10% horse serum (HS) and Pen-Strep 1% were purchased from Gibco BRL, Gaithersburg, MD, U.S.A. 50 U ml^{-1} of recombinant mouse γ-interferon were purchased from (IFN, Genzyme, Cambridge, MA, U.S.A.). Opti-MEM I reduced serum medium was purchased from Thermo Fisher Scientific, Waltham, Massachusetts, U.S.A. 50 ng ml^{-1} of nerve growth factor (NGF) was purchased from Sigma Aldrich, Milan, Italy.

4.2. Hybrid nanocomposites

The PVDF/BT nanocomposite was prepared by dissolving 30 g of PVDF powder in 200 mL of DMF. The mixture was stirred in a water bath at 70 °C overnight until a clear and transparent solution formed. 10 wt% of BT nanoparticles were dispersed in 50 mL of DMF using a probe sonicator for 60 minutes under nitrogen flow at 0 °C. This dispersed BT was added to the PVDF solution and then sonication was conducted for a duration of 30 minutes in an environment of nitrogen flow at a temperature of 0 °C, followed by stirring for 2 hours to form a stable suspension. The suspension was poured onto a pristine glass plate and allowed to air dry, leaving it to evaporate at room temperature. The film extracted from the dish was delicately separated and subsequently cut into small pieces, and finely ground before being fed into the extruder machine. More details about different BT concentrations are available in our previous work.[34]

The synthesis of graphene oxide (GO) involved the utilization of natural graphite powder through a customized Hummers' method, following a documented protocol.[67] To prepare the PVDF/rGO composite, PVDF was dissolved in DMF, and rGO was added at a 0.5 wt% loading. To achieve a uniform distribution of rGO nanosheet within the polymer matrix, the mixture was subjected to additional stirring and sonication for two hours. After the solvent evaporation step, the resulting composite material was fragmented into smaller pieces and then subjected to an ethanol wash. Subsequently, it was placed in a vacuum oven preheated to 60 °C and allowed to dry for 3 hours. The composite material was subsequently finely powdered through manual grinding using a mortar while being

cooled with liquid nitrogen. More details are available in our previous work.[35]

4.3. Melt spinning of nanocomposite piezoelectric filaments

Nanocomposite filaments were manufactured utilizing a twin-screw extruder sourced from Barrel Scientific Ltd through the melt-spinning technique. Monofilaments were fabricated using a spinneret with a single 3 mm dimeter die size. To maintain consistent filament diameter, the flow volume of composites through the spinneret was controlled. The extruder comprised nine consecutive zones with temperature profiles ranging from 180 to 220 °C. For more details, refer to our previous work.[36]

4.4. Characterization

FTIR spectra spanning 400 to 4000 cm^{-1} were recorded for both pristine PVDF fibers and PVDF/BT nanocomposite fibers. This analysis was performed by Shimadzu IR Prestige-21 Spectrometer in ATR mode. The diameter of each fiber was assessed at ten different locations along their lengths using image J software. The Shimadzu tensile tester (EZ-S) was employed to evaluate the mechanical properties of the filaments. The specimens were clamped between two grips and underwent tensile testing at a constant rate of 10 mm min^{-1}. The TRAPEZIUMX software recorded the mechanical properties of each fiber. The same setup was used to stretch the coil structures to specific strains. The electrical response of the piezoelectric sample was evaluated using a Picoscope 4424 digital oscilloscope (Pico Technology) and Keithley (2612B, USA). The surface characteristics of fibers were analyzed using a JEOL 7500 scanning electron microscope (SEM). The reported data for all measured samples are based on average values, with at least five measurements taken for each sample.

4.5. Cytocompatibility test

Human adipose tissue harvesting. The use of adipose stromal cells in this study was based on the approval from the Medical Ethics Committee in University Malaya Medical Centre (reference number: 20149-563). Adipose tissue samples were collected each from donors (obtained written informed consents) who undergoing orthopaedic-related surgeries ($N = 8$; mean age = 64.7 years).

Isolation and culture of human adipose derived-MSCs. Human adipose-derived mesenchymal stromal cells (AD-MSCs) were isolated using the protocol established in our laboratory.[49] Briefly, the harvested adipose tissue sample was minced and digested with type I collagenase for 1 hour. The centrifuged cell pellet containing stromal vascular fraction (SVF) was collected and cultured with complete cell growth medium (low-glucose DMEM supplemented with 10% fetal bovine serum, 1% GlutaMAX™-I, 1% penicillin–streptomycin) (Invitrogen-Gibco, USA), and incubated at 37 °C in a humidified 5% CO_2 incubator. The 80% confluency cells were sub-cultured until passage 3 for further experiments.

Cell seeding on fabricated scaffold. The sheet scaffold and coiled string scaffold were cut into the size of 1 cm × 1 cm and 1 cm length, respectively. The cut scaffolds were thoroughly rinsed with 70% ethanol and sterile 1× phosphate-buffered saline (PBS; pH 7.4) (Invitrogen-Gibco, USA) prior to cell seeding. The passaged-3 AD-MSCs were harvested and counted using a trypan blue (Invitrogen-Gibco, USA) exclusion test. A total of 2 × 104 cells were then seeded onto each scaffold and allowed to attach for 24 hours. The cells were then continued to be cultured for 1, 7, and 14 days, for further experiments.

Cell proliferation and viability. To evaluate the biocompatibility of scaffolds and viability of cells on the scaffolds, cell proliferation on the scaffold was performed using the alamarBlue® (AB) (Invitrogen-Gibco, USA) assay, which is based on the colorimetric quantitative analytical principle. At day 1, 7, and 14 after cells attachment, 1/10th volume AB reagent was added to samples in culture medium and incubated in dark at 37 °C. Following a 4-hour incubation, the absorbance of the aliquot was gauged at 570 nm, with 600 nm utilized as the reference wavelength. Adhering to the manufacturer's protocol, the AB reduction percentage was computed, with background values corrected using medium without cells.

Cell adhesion and morphology. The Quanta™ FEG 650 FESEM instrument from FEI, USA, was employed to analyze cell attachment and morphology on the scaffolds. Specimens were fixed in 4% glutaraldehyde at 4 °C overnight at each time point. Following fixation, they underwent dehydration using a gradient of ethanol concentrations and were subsequently dried *via* critical point drying. The dried samples were sputter-coated with gold before viewing under a scanning electron microscope.

To examine the cell distribution on the scaffold, the sheet scaffold seeded with cells were fixed with 3.7% paraformaldehyde in PBS and the nuclei were stained with Hoechst 33342 blue dye (Molecular Probes, USA). The stained samples were imaged by using confocal microscopy system (Leica TCL SL, Germany) after 30 min incubation at room temperature.

Osteogenic properties. At the day 14, the sheet scaffold samples were examined for osteogenic differentiation potential. Osteocalcin (OCN) production in the samples was determined using an ELISA kit (Elabscience®, USA) by detecting the sandwich antibody–antigen complex in the lysate solution, following the manufacturer's protocol. The absorbance was measured at a 450 nm wavelength and analysed using established standard curve. The matrix mineralization was determined *via* quantitative analysis with alizarin red-S staining performed by determining absorbance values. Briefly, the scaffolds with cells were stained with 2% aqueous alizarin red S, the solution dye was then extracted and measured at a wavelength of 562 nm.

Statistical analysis. Bioactivity assays were performed with technical triplicates (n) per experimental run, utilizing four independent samples from distinct donors (N) per group. Data is expressed as mean ± standard deviation (SD), with Student's t-test employed to assess differences in mean values. A confidence level of 95% ($p < 0.05$) was chosen for determining statistical significance using the SPSS version 23 software (SPSS Inc., USA).

Data availability

The data supporting this article have been included as part of the ESI.† Any additional information can be obtained from the corresponding author upon reasonable request.

Conflicts of interest

The authors declare no conflict of interest.

Acknowledgements

F. M. acknowledges financial support received from Deakin University through Alfred Deakin Postdoctoral Research Fellowship (2022). N. H. Y. acknowledges financial support received by University Malaya Impact Oriented Interdisciplinary Research Grant (IIRG002-2022FNW). The authors would like to thank Peggy Kong for her assistance with the cells work. The authors acknowledge the financial support received from Hannover Medical School through the Department of Cardiothoracic, Transplantation, and Vascular Surgery.

References

1 K. Chen, J. Ren, C. Chen, W. Xu and S. Zhang, *Nano Today*, 2020, **35**, 100939.
2 M. Sawane and M. Prasad, *Mater. Sci. Semicond. Process.*, 2023, **158**, 107324.
3 F. Hahn, A. Ferrandez-Montero, M. Queri, C. Vancaeyzeele, C. Plesse, R. Agniel and J. Leroy-Dudal, *ACS Appl. Mater. Interfaces*, 2024, **16**, 5613–5626.
4 I. Rocha, G. Cerqueira, F. Varella Penteado and S. I. Córdoba de Torresi, *Front. Med. Technol.*, 2021, **3**, 670274.
5 T.-L. Yang, Y.-C. Hsiao, S.-J. Lin, H.-W. Lee, P.-J. Lou, J.-Y. Ko and T.-H. Young, *Biomaterials*, 2010, **31**, 288–295.
6 T.-H. Young, J.-N. Lu, D.-J. Lin, C.-L. Chang, H.-H. Chang and L.-P. Cheng, *Desalination*, 2008, **234**, 134–143.
7 B. Guo and P. X. Ma, *Biomacromolecules*, 2018, **19**, 1764–1782.
8 B. Tschoeke, T. C. Flanagan, A. Cornelissen, S. Koch, A. Roehl, M. Sriharwoko, J. S. Sachweh, T. Gries, T. Schmitz-Rode and S. Jockenhoevel, *Artif. Organs*, 2008, **32**, 800–809.
9 J. Li, Y. Long, F. Yang and X. Wang, *Curr. Opin. Solid State Mater. Sci.*, 2020, **24**, 100806.
10 F. Mokhtari, J. Foroughi and M. Latifi, Energy Harvesting Properties of Electrospun Nanofibers, *IOP Publishing Ltd 2020*, 2019, 5, DOI: **10.1088/978-0-7503-2005-4ch5**.
11 F. Mokhtari, Z. Cheng, C. H. Wang and J. Foroughi, *Global Challenges*, 2023, **7**, 2300019.
12 S. Chen, P. Zhu, L. Mao, W. Wu, H. Lin, D. Xu, X. Lu and J. Shi, *Adv. Mater.*, 2023, **35**, 2208256.
13 F. Xie, X. Qian, N. Li, D. Cui, H. Zhang and Z. Xu, *Ann. Transl. Med.*, 2021, **9**, 880.
14 C. Hu, K. Behdinan and R. Moradi-Dastjerdi, *Actuators*, 2022, **11**, 187.
15 A. Kumar, R. Kiran, S. Kumar, V. S. Chauhan, R. Kumar and R. Vaish, *Global Challenges*, 2018, **2**, 1700084.
16 F. Mokhtari, M. Salehi, F. Zamani, F. Hajiani, F. Zeighami and M. Latifi, *Text. Prog.*, 2016, **48**, 119–219.
17 G. de Marzo, V. M. Mastronardi, L. Algieri, F. Vergari, F. Pisano, L. Fachechi, S. Marras, L. Natta, B. Spagnolo, V. Brunetti, F. Rizzi, F. Pisanello and M. De Vittorio, *Adv. Electron. Mater.*, 2023, **9**, 2200069.
18 Y. Guo, C. Liu, H. Liu, W. Wang, H. Li and C. Zhang, *Polym. Degrad. Stab.*, 2021, **193**, 109722.
19 B. Azimi, M. Milazzo, A. Lazzeri, S. Berrettini, M. J. Uddin, Z. Qin, M. J. Buehler and S. Danti, *Adv. Healthcare Mater.*, 2020, **9**, e1901287.
20 F. Mokhtari, B. Azimi, M. Salehi, S. Hashemikia and S. Danti, *J. Mech. Behav. Biomed. Mater.*, 2021, **122**, 104669.
21 F. Mokhtari, Z. Cheng, R. Raad, J. Xi and J. Foroughi, *J. Mater. Chem. A*, 2020, **8**, 9496–9522.
22 T. Vijayakanth, S. Shankar, G. Finkelstein-Zuta, S. Rencus-Lazar, S. Gilead and E. Gazit, *Chem. Soc. Rev.*, 2023, **52**, 6191–6220.
23 L. Wang, K. Jiang and G. Shen, *Adv. Mater. Technol.*, 2021, **6**, 2100107.
24 F. Mokhtari, M. Shamshirsaz, M. Latifi and J. Foroughi, *Polymers*, 2020, **12**, 2697.
25 X. Cheng, X. Xue, Y. Ma, M. Han, W. Zhang, Z. Xu, H. Zhang and H. Zhang, *Nano Energy*, 2016, **22**, 453–460.
26 S. Azimi, A. Golabchi, A. Nekookar, S. Rabbani, M. H. Amiri, K. Asadi and M. M. Abolhasani, *Nano Energy*, 2021, **83**, 105781.
27 A. Khan, R. Joshi, M. K. Sharma, A. Ganguly, P. Parashar, T.-W. Wang, S. Lee, F.-C. Kao and Z.-H. Lin, *Nano Energy*, 2024, **119**, 109051.
28 A. Wang, Z. Liu, M. Hu, C. Wang, X. Zhang, B. Shi, Y. Fan, Y. Cui, Z. Li and K. Ren, *Nano Energy*, 2018, **43**, 63–71.
29 F. Mokhtari, S. Danti, B. Azimi, F. Hellies, E. Zanoletti, G. Albertin, L. Astolfi, R. J. Varley and J. M. Razal, *Energy Environ. Mater.*, 2024, e12807.
30 H. Takise, M. Suzuki, T. Takahashi and S. Aoyagi, *Int. J. Nanotechnol.*, 2018, **15**, 900–913.
31 H. Park, H. Si, J. Gu, D. Lee, D. Park, Y.-I. Lee and K. Kim, *Sci. Rep.*, 2023, **13**, 2582.
32 F. Gaßdorf, Z. Fan, J. Schwaderer, S. Beuermann, R. Wilhelm, A. P. Weber and M. Fischlschweiger, *Macromol. Rapid Commun.*, 2023, **44**, 2300177.
33 M. N. Islam, R. H. Rupom, P. R. Adhikari, Z. Demchuk, I. Popov, A. P. Sokolov, H. F. Wu, R. C. Advincula, N. Dahotre, Y. Jiang and W. Choi, *Adv. Funct. Mater.*, 2023, **33**, 2302946.
34 F. Mokhtari, G. M. Spinks, C. Fay, Z. Cheng, R. Raad, J. Xi and J. Foroughi, *Adv. Mater. Technol.*, 2020, **5**, 1900900.
35 F. Mokhtari, G. M. Spinks, S. Sayyar, Z. Cheng, A. Ruhparwar and J. Foroughi, *Adv. Mater. Technol.*, 2021, **6**, 2000841.
36 F. Mokhtari, J. Foroughi, T. Zheng, Z. Cheng and G. M. Spinks, *J. Mater. Chem. A*, 2019, **7**, 8245–8257.
37 K. Pilla, M. Neergat and K. N. Jonnalagadda, *J. Polym. Sci.*, 2023, **61**, 1082–1096.
38 C. Shuai, Z. Zeng, Y. Yang, F. Qi, S. Peng, W. Yang, C. He, G. Wang and G. Qian, *Mater. Des.*, 2020, **190**, 108564.
39 I. O. Pariy, A. A. Ivanova, V. V. Shvartsman, D. C. Lupascu, G. B. Sukhorukov, T. Ludwig, A. Bartasyte, S. Mathur, M. A. Surmeneva and R. A. Surmenev, *Polymers*, 2019, **11**, 1065.

40 M. Kubin, P. Makreski, M. Zanoni, L. Gasperini, G. Selleri, D. Fabiani, C. Gualandi and A. Bužarovska, *Polym. Test.*, 2023, **126**, 108158.
41 N. Dilip Kulkarni, M. Kumar and P. Kumari, *Mater. Today: Proc.*, 2023, **76**, 81–87.
42 F. Mokhtari, *Self-Powered Smart Fabrics for Wearable Technologies*, Springer Nature, 2022.
43 C. Ning, Z. Zhou, G. Tan, Y. Zhu and C. Mao, *Prog. Polym. Sci.*, 2018, **81**, 144–162.
44 A. Karunanithi, T. Y. Suryawanshi, N. Redkar, P. K. S. Mural, S. Saxena and S. Shukla, *Environ. Sci.: Water Res. Technol.*, 2023, **9**, 2891–2902.
45 S. Pei, F. Ai and S. Qu, *RSC Adv.*, 2015, **5**, 99841–99847.
46 N. Abzan, M. Kharaziha and S. Labbaf, *Mater. Des.*, 2019, **167**, 107636.
47 T. Liu, Y. Wang, M. Hong, J. Venezuela, W. Shi and M. Dargusch, *Nano Today*, 2023, **52**, 101945.
48 C. Liao, Y. Li and S. C. Tjong, *Int. J. Mol. Sci.*, 2018, **19**, 3564.
49 H. Y. Nam, M. R. Draman Yusof and T. Kamarul, *Stem Cells Int.*, 2023, **2023**, 4907230.
50 M. Ouzin and G. Kogler, *Cells*, 2023, **12**, 2039.
51 K. Czerwiec, M. Zawrzykraj, M. Deptuła, A. Skoniecka, A. Tymińska, J. Zieliński, A. Kosiński and M. Pikuła, *Int. J. Mol. Sci.*, 2023, **24**, 3888.
52 P. Bellet, M. Gasparotto, S. Pressi, A. Fortunato, G. Scapin, M. Mba, E. Menna and F. Filippini, *Nanomaterials*, 2021, **11**, 404.
53 E. Zeimaran, S. Pourshahrestani, H. Y. Nam, N. A. B. Abd Razak, K. Kalantari, T. Kamarul, B. Salamatinia and N. A. Kadri, *React. Funct. Polym.*, 2020, **154**, 104668.
54 Y. Huang, Q. Li, K. Zhang, M. Hu, Y. Wang, L. Du, L. Lin, S. Li, L. Sorokin, G. Melino, Y. Shi and Y. Wang, *Cell Death Dis.*, 2019, **10**, 368.
55 S. Baig, A. H. S. Azizan, H. R. B. Raghavendran, E. Natarajan, S. Naveen, M. R. Murali, H. Y. Nam and T. Kamarul, *Stem Cells Int.*, 2019, **2019**, 5142518.
56 K. Ng, P. Azari, H. Y. Nam, F. Xu and B. Pingguan-Murphy, *Polymers*, 2019, **11**, 650.
57 H. Y. Nam, M. R. Murali, R. E. Ahmad, B. Pingguan-Murphy, H. R. B. Raghavendran and T. Kamarul, *Stem Cells Int.*, 2020, **2020**, 5385960.
58 E. Vardar, H. Y. Nam, G. Vythilingam, H. L. Tan, H. A. Mohamad Wali, E. M. Engelhardt, T. Kamarul, P. Y. Zambelli and E. Samara, *Int. J. Mol. Sci.*, 2023, **24**, 16945.
59 D. D'Alessandro, C. Ricci, M. Milazzo, G. Strangis, F. Forli, G. Buda, M. Petrini, S. Berrettini, M. J. Uddin and S. Danti, *Biomolecules*, 2021, **11**, 1731.
60 A. Carter, K. Popowski, K. Cheng, A. Greenbaum, F. S. Ligler and A. Moatti, *Bioelectricity*, 2021, **3**, 255–271.
61 A. Lund, K. Rundqvist, E. Nilsson, L. Yu, B. Hagström and C. Müller, *npj Flexible Electron.*, 2018, **2**, 9.
62 D. Yun, J. Park and K.-S. Yun, *Electron. Lett.*, 2015, **51**, 284–285.
63 N. Soin, T. H. Shah, S. C. Anand, J. Geng, W. Pornwannachai, P. Mandal, D. Reid, S. Sharma, R. L. Hadimani, D. V. Bayramol and E. Siores, *Energy Environ. Sci.*, 2014, **7**, 1670–1679.
64 S. K. Karan, R. Bera, S. Paria, A. K. Das, S. Maiti, A. Maitra and B. B. Khatua, *Adv. Energy Mater.*, 2016, **6**, 1601016.
65 W. Zeng, X.-M. Tao, S. Chen, S. Shang, H. L. W. Chan and S. H. Choy, *Energy Environ. Sci.*, 2013, **6**, 2631–2638.
66 F. Mokhtari, G. M. Spinks, S. Sayyar and J. Foroughi, *Nanomaterials*, 2021, **11**, 2153.
67 S. Sayyar, E. Murray, B. C. Thompson, S. Gambhir, D. L. Officer and G. G. Wallace, *Carbon*, 2013, **52**, 296–304.